Interfaces between buckling phases in silicene: *Ab initio* density functional theory calculations

Matheus P. Lima,[1,*] A. Fazzio,[1,†] and Antônio J. R. da Silva[1,2,‡]

[1]*Instituto de Física, Universidade de São Paulo, CP 66318, 05315-970 São Paulo, São Paulo, Brazil*

[2]*Laboratório Nacional de Luz Síncrotron, CP 6192, 13083-970 Campinas, São Paulo, Brazil*

(Received 15 June 2013; revised manuscript received 25 October 2013; published 10 December 2013)

The buckled structure of silicene leads to the possibility of new kinds of line defects that separate regions with reversed buckled phases. In the present work we show that these new grain boundaries have very low formation energies, one order of magnitude smaller than grain boundaries in graphene. These defects are stable along different orientations, and they can all be differentiated by scanning tunneling microscopy images. All these defects present local dimerization between the Si atoms, with the formation of π bonds. As a result, these defects are preferential adsorption sites when compared to the pristine region. Thus, the combination of low formation energy and higher reactivity of these defects may be cleverly used to design new nanostructures embedded in silicene.

DOI: 10.1103/PhysRevB.88.235413 PACS number(s): 61.72.−y, 61.46.−w, 31.15.E−

I. INTRODUCTION

The first in-lab observation of silicene[1] has attracted the attention of the community that studies new materials due to their similarities with graphene.[2] For this reason, efforts have been employed to understand and control the growth of silicene.[3–8] These experimental measurements confirmed some theoretical predictions done several years before.[9,10] Recent works have suggested that silicene is a potential candidate for applications in nanoelectronics.[11] However, having in mind device development and integration, it is fundamental to have a deep understanding of the influences that defects, doping, interactions with substrates, external fields, and magnetic moments have on the properties of this material in order to fully exploit the possibilities of silicene in nanotechnology. Currently, these tasks represent great challenges and the necessary knowledge is still in its infancy.

When compared to graphene, silicene has a new and important ingredient: the presence of a buckled structure. The understanding of the effects caused by this extra feature is crucial to explore the full potential of this material. Few consequences of this buckling pattern have already been investigated; among them we can mention (i) the increase of spin-orbit coupling, enhancing the quantum spin Hall effect;[12] (ii) the possibility to tune the energy gap and the topological phase by the application of an external electric field perpendicular to the sheet;[13–15] and (iii) the increase of the surface reactivity.[16]

Due to the buckling, there are, in fact, two equivalent energy degenerate geometric phases (α and β) in silicene. The α phase has a given atom shifted up and its first neighbors shifted down, whereas in the β phase the shifts are reversed. A new possibility is thus the coexistence of both the α and β phases in the same sample. This situation may be created by different causes, such as a peculiar growth mechanism or the interaction with the substrate, since such interactions may pin down particular phases in different regions of the sample.

In this article we investigate these new kinds of line defects created at the interface between the α and β phases in silicene. These buckling phase interfaces may occur along different orientations (zigzag, armchair, or intermediated chiral geometries) and have a much lower energy than grain boundaries in graphene. The main characteristic of such defects is the presence of π bonds between the interface atoms caused by an out-of-plane dislocation rearrangement. For the zigzag direction, the formation of π bonds is more clear, leading to a slightly lower formation energy when compared to any other directions. We analyze in detail how these interfaces could be observed and differentiated in scanning tunneling microscopy (STM) images. Furthermore, we show that the reactivity is enhanced at these interface regions, exemplified by demonstrating that Au atoms have a lower binding energy when adsorbed over these buckling phase interfaces in comparison with the pristine regions.

II. COMPUTATIONAL DETAILS

Our results were obtained with *ab initio* density-functional theory calculations. We used the SIESTA code[17] within the local-density approximation[18] (LDA) for the exchange-correlation functional. Two-dimensional (2D) periodic boundary conditions were employed in all calculations, with a grid of 50×50 k points in the unit cell, a double-ζ polarized basis, and a mesh cutoff of 300 Ry to define the grid in the real space. A vacuum of 20 Å is sufficient to avoid undesirable interactions between the periodic images of silicene sheets. For the pristine system we obtain a lattice constant of 3.854 Å, bond lengths of 2.281 Å, and out-of-plane dislocations of ± 0.25 Å. These parameters are consistent with earlier results found in the literature.[9,19,20] We also calculated a barrier of 35 meV/atom to revert the buckling phase in the whole system.

The simulations of linear defects are done with two complementary interfaces to reach the 2D periodicity in the sheet plane. To generate fully relaxed geometries we first take a supercell with the pristine geometry. Subsequently, we revert the out-of-plane dislocation only in a certain region where we wish to observe the inverted phase. Subsequently, we perform a fully conjugate gradient relaxation using a force criterion of 0.015 eV/Å to quench the forces in the whole system. As expected, the major modifications will occur only close to the phase interface.

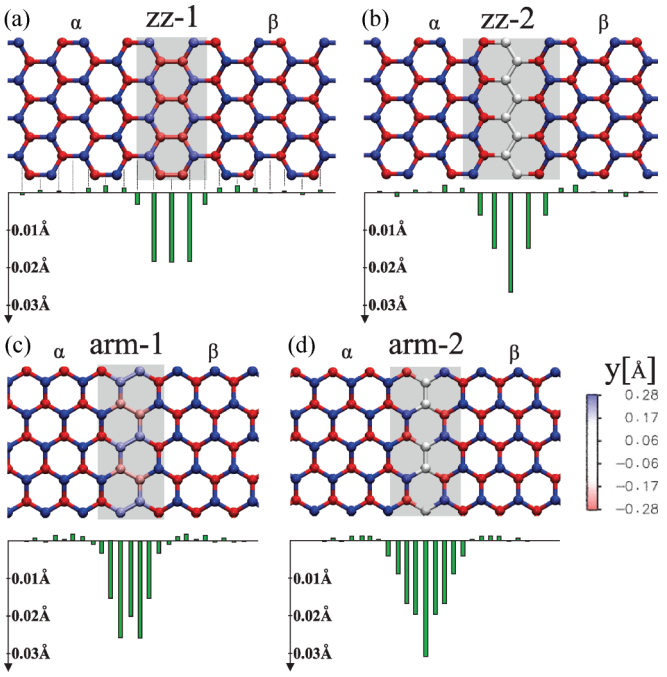

FIG. 1. (Color online) Fully relaxed geometries for the (a) zz-1 interface in the zigzag direction, (b) zz-2 interface in the zigzag direction, (c) arm-1 interface in the armchair direction, and (d) arm-2 interface in the armchair direction. The atoms are colored according to their out-of-plane dislocation (y). The gray rectangles emphasize the interface region. Below each structure are presented the bond-length deviations from the pristine silicene ($d^{\text{bulk}} - d$).

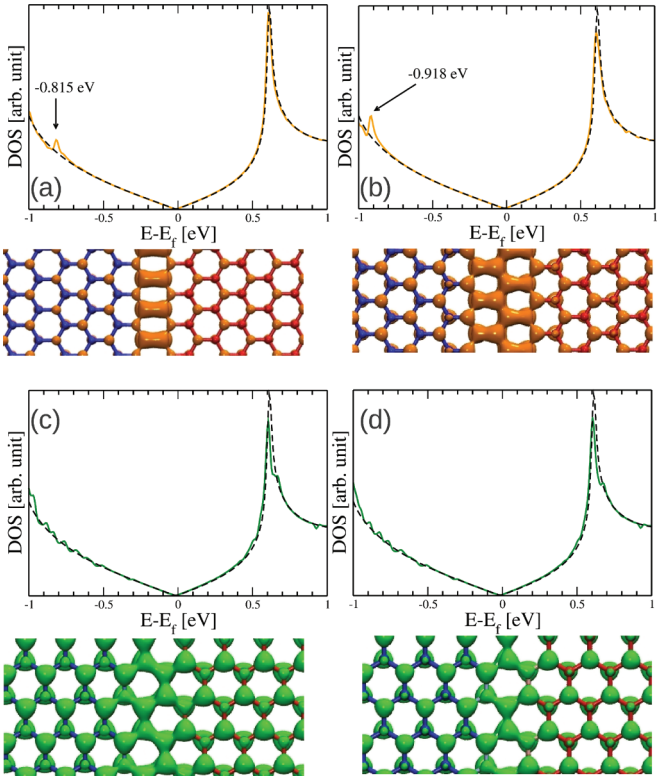

FIG. 2. (Color online) DOS and LDOS for the α-β interfaces: (a) zz-1, (b) zz-2, (c) arm-1, and (d) arm-2. For (a) and (b) the LDOS were calculated around the peaks localized at -0.814 and -0.918 eV below the Fermi energy, respectively. An energy window of ± 0.025 eV was adopted. For (c) and (d) the LDOS were calculated integrating the states within the energy range $-0.9 \leqslant E - E_f \leqslant -0.4$ eV.

III. RESULTS

A. Fully relaxed geometries

The fully relaxed geometries (which remain planar) for the interfaces considered in this work are shown in Fig. 1.[21] We considered four kinds of interfaces, two along the zigzag direction and two along the armchair direction. In Fig. 1(a) we show the zz-1 interface along the zigzag direction, which has pairs of neighboring atoms with the same out-of-plane dislocation (y). In Fig. 1(b) we show the zz-2 interface along the zigzag direction. In this case, there is a line of zigzagged atoms with $y = 0$. Figure 1(c) depicts the arm-1 interface, which occurs along the armchair direction. Here, the interface atoms form a line with dimerized out-of-plane dislocations, which means two atoms with positive out-of-plane dislocations followed by two atoms with negative out-of-plane dislocations. Figure 1(d) depicts the arm-2 interface along the armchair direction. There are pairs of neighboring atoms with $y = 0$ at this interface. Below each structure we present the bond-length variation from the pristine distance. Although the interfacial atoms have a bond length around 0.03 Å shorter than the pristine atoms, the interatomic distances are quickly reestablished as one moves away from the line defect. Such analysis allows one to conclude that the width of these line defects is not more than 7 Å.

B. Electronic structure

Aiming to understand the influences of such line defects in the electronic structure of silicene, we calculated the density of states (DOS) within an energy window of ± 1 eV around the Fermi energy. We present the results in Fig. 2. For the zz-1 interface, shown in Fig. 2(a), the DOS is very similar to the pristine case, with the exception of a sharp peak localized at -0.815 below the Fermi energy (E_f). The local density of states (LDOS) calculated within an energy window of ± 0.025 eV centered at this peak is shown below its DOS. This LDOS reveals that this peak is primarily composed by states with a π-bond signature localized at the interface atoms. The narrow shape of this resonance peak indicates that the zz-1 defect levels have a small dispersion as well as a small coupling to the rest of the system. In Fig. 2(b) we present the results for the zz-2 interface. Again, only a sharp peak is present in the DOS; however, its energy is lower (-0.918 eV), and its amplitude is higher. Similarly to the zz-1 case, the LDOS centered at this peak allows us to conclude that these states have a π bond signature and a small coupling to the rest of the system. Therefore, the creation of both kinds of zigzag defects leads to the formation of π states localized at the interface atoms.

To better illuminate the understanding about the influence of such linear defects in the electronic structure of silicene, we modeled the system with an effective first nearest-neighbor tight-binding (TB) Hamiltonian, given by

$$H = \sum_{\langle i,j \rangle} -t c_i^\dagger c_j + \sum_i U_i c_i^\dagger c_i + \text{H.c.} \qquad (1)$$

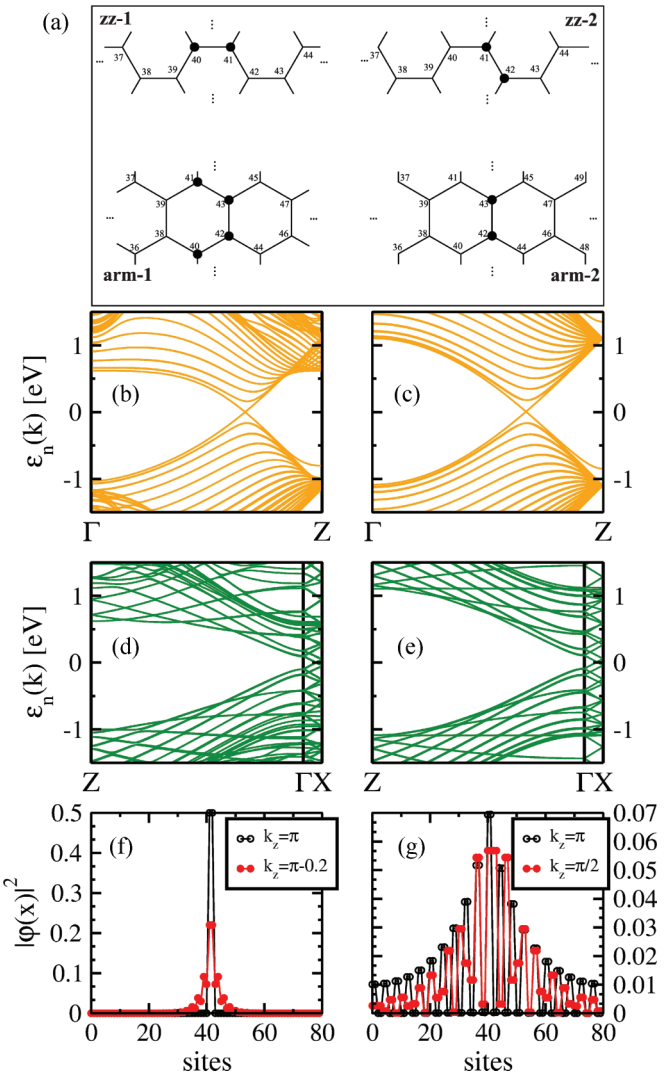

FIG. 3. (Color online) (a) Black circles highlighting the rehybridized sites where U_i must be modified for the zz-1, zz-2, arm-1, and arm-2 defects. Energy bands are for the zz-1 structure calculated with (a) DFT and (b) our tight-binding model; (c) and (d) show similar calculations for the arm-1 structure. Tight-binding wave functions for the highest occupied energy band ($k_x = 0$) for the (e) zz-1 and (f) arm-1 structures. Here, the tight-binding calculations consider a total of 80 sites ($N = 80$).

$c_i^\dagger$ (c_i) creates (annihilates) an electron at the site i, t is the transfer integral, and U_i is the on-site energy.

Considering this model, the main effects caused by the buckling phase inversion are changes in the on-site energy U_i only for the interfacial atoms due to the local rehybridization occurring at them.[22] However, note that the disposition of these interfacial atoms is distinct for each structure. In Fig. 3(a) we mark with black circles the rehybridized sites where U_{site} must be modified. We adjust the tight-binding parameters to better fit with the energy bands calculated with DFT.

In Figs. 3(b) and 3(c) we compare the DFT and TB energy bands for the zz-1 interface, respectively. Despite some discrepancies far from E_f, the general behavior is essentially the same for both DFT and TB calculations. For this defect, the adjusted parameters are $t = 1.1$ eV and $U_i = 0.25t$ ($U_i = 0$ for bulk atoms). The positive value of U_i brings the defect states to the top of the occupied energy bands. Analyzing the Hamiltonian (see Appendix A), it is possible to note that the effective couplings of the defect atoms highlighted in Fig. 3(a) to the rest of the system have the form of $-t(1 + e^{\pm ik_z})$ and are thus negligible close to $k_z = \pi$. The modulus square of the TB wave function at $k_z = \pi$ is depicted in Fig. 3(f) and can be clearly seen to be a strictly localized wave function. For other values of k_z, the states progressively become more dispersive as a consequence of the increasing of the effective coupling of the defect sites to the rest of the system. The wave function for $k_z = \pi - 0.2$ is also depicted in Fig. 3(f), and a non-null contribution of the neighboring sites induced by the increase of the effective coupling term is present.

We also compare, in Figs. 3(d) and 3(e), the DFT and TB results for the arm-1 defect, respectively. Here, the adjusted parameters are $t = 1.1$ eV and $U_i = 0.15t$. Again, there is a great overall agreement between the results calculated with both methods, and due to the positive value of U_i the defect states once again lie at the top of the highest occupied band. However, contrary to the zigzag direction, in the armchair direction the effective coupling between the defect sites and the rest of the system never vanishes for any $\vec{k}$ point. We illustrate this behavior in Fig. 3(g), where we show the modulus square of the wave function for $k_z = \pi$ and $\pi/2$. It can be clearly seen that, even though the states are more localized at the defect sites, a contribution at sites of distant neighbors is present. The numerical TB results also indicate that the states at the central region of the valence band (around $k = \pi/2$) are slightly more localized than the states close to Γ and Z.

Now, let us focus again on the results obtained with calculations based on DFT. The DOS are presented in Figs. 2(c) and 2(d) for the arm-1 and arm-2 interfaces, respectively. The behavior is quite similar for both armchair interfaces: (i) there are no peaks associated with any localized states and (ii) the DOS are very similar to the pristine case, except for small oscillations caused by the interaction between the line defects and its complementary images (see Appendix B). Since our TB model indicates that the defect states are mainly localized at the central part of the valence band, we calculated the LDOS for an energy range from $E - E_f = -0.9$ to -0.4 eV, for both arm-1 and arm-2 cases. In both cases, it is possible to see a slightly greater contribution of the defect sites, even considering that the defect levels are weakly localized, and some bulk states have been included in this LDOS.

An important remark to be made is that, even though these interfaces create defect states at the top of the highest occupied energy band, close to E_f they are always delocalized. As a result, the modifications in the DOS very close to the Fermi level in all cases are negligible. For example, the Dirac cone characteristic V shape is fully maintained. Even with the inclusion of the spin-orbit coupling in the calculations, the differences between the pristine and the defective systems are negligible around E_f. Therefore, these defects will be quasi invisible to measurements that depend solely on the Fermi surface.

C. Simulations of scanning tunneling microscope images

We show in Fig. 4 that it is possible to differentiate the various interfaces with scanning tunneling microscopy

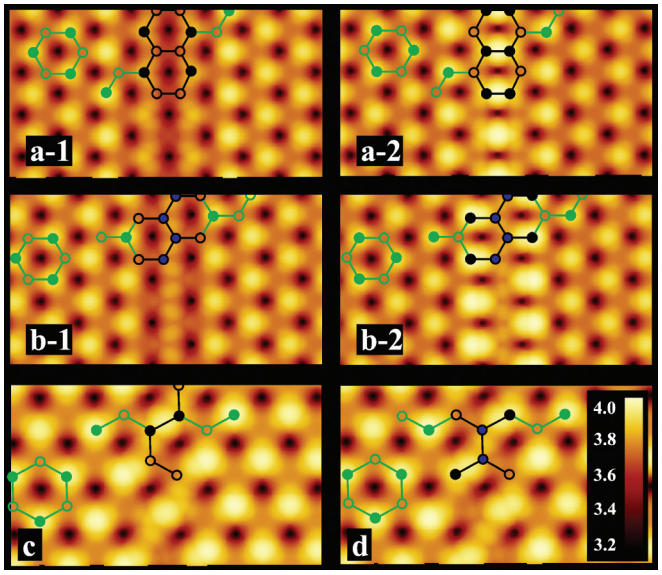

FIG. 4. (Color online) Images of the STM simulations for the buckling phase interfaces: (a-1) and (a-2) zz-1 interface, (b-1) and (b-2) zz-2 interface, (c) arm-1 interface, and (d) arm-2 interface. The filled (nonfilled) circles represent Si atoms with up (down) shifts. The lines are guides to the eye. The scale bar represent the tip height in Å.

(STM) images. We used the Tersoff-Ramann theory,[23] with a bias voltage of 1.0 V, considering occupied states and the constant current model. STM images were commonly used to experimentally investigate silicene.[1,3–8] Similarly to the experiments, our simulations show a clear signature of the buckling pattern at the pristine region: the signal presents high spots over the up-shifted atoms, low spots over the down-shifted atoms, and absence of signal at the center of the hexagons.[24] For the buckling interfaces, the out-of-plane displacements create distinct patterns depending on the interface symmetry, as shown in detail in Fig. 4. In Fig. 4(a-1) we present the STM image for the zz-1 interface. The positions of the interface atoms are indicated by black circles. In this picture, there is a clear line of low signals along the dimerized central interface atoms because they are down-shifted with respect to the STM tip. If we consider the other possible orientation of the STM tip, these same atoms would now be up-shifted, and we would obtain a line of high signals, as shown in Fig. 4(a-2). An interesting feature of this image is the clear signal of π bonds between the central atoms of the defect. For the zz-2 interface there are also two possible images, depending on the tip orientation. These images are shown in Figs. 4(b-1) and 4(b-2). Here, the source of the differences is the fact that all first-neighbor atoms to the interface atoms have the same out-of-plane dislocation. Well-defined π bonds can also be identified between interface atoms and their first neighbors via STM images.

For the interfaces in the armchair direction, differently from those in the zigzag direction, the STM images do not depend on the tip orientation, as shown in Figs. 4(c) and 4(d) for the arm-1 and arm-2 interfaces, respectively. In both cases, the out-of-plane rearrangement can be clearly inferred from STM images, and the π bonds can also be detected. Thus, we have shown that it is experimentally possible to use STM images to identify and differentiate all these distinct interfaces.

TABLE I. Formation energy per unity length (U^{form} in meV/Å) for the line defects considered in this work.

	zz-1	zz-2	Arm-1	Arm-2	$\theta = 19.11^\circ$
U^{form}	17.5	17.9	20.9	20.3	22.8

D. Formation energies

The formation energies per unity length (U^{form}) for all the defects are presented in Table I. The interfaces along the zigzag direction have the lowest formation energies, because the π bonds are more clearly formed, leading to a slightly larger energy gain. Otherwise, the two zigzag and the two armchair interfaces have formation energies quite similar among themselves. Besides the zigzag and armchair directions, we also consider one intermediate case, with an angle $\theta = 19.11^\circ$ with the zigzag direction. The fully relaxed geometry is shown in Fig. 5, where it can be seen that the rearrangement of the out-of-plane dislocations is more complex, leading to a higher formation energy due to the increase of the elastic contribution. We expect the same behavior for other chiral angles.

The values of U_{form} presented in Table I indicate that the defects in the zigzag direction will be more easily created at low temperatures. Indeed, a recent work by Chen *et al.* reports a spontaneous symmetry-breaking phase transition in silicene over the Ag(111) substrate.[27] They have shown, at low temperatures, a spontaneous creation of a 2D grid where the domains are triangles with alternating buckling phases separated by interfaces in the zigzag direction. Although the authors did not discuss the structural details of the triangles borders, it can be inferred from their STM images that they are the zz-2 interfaces described above. It is important to note that the particular triangular structure observed experimentally will most likely depend on the interaction between the silicene and the Ag substrate. This indicates that on the one hand the defects that we propose are very likely to be observed but on the other hand the particular configuration that they will have on the silicene sheet will depend on experimental details such as substrate configuration and growth temperature.

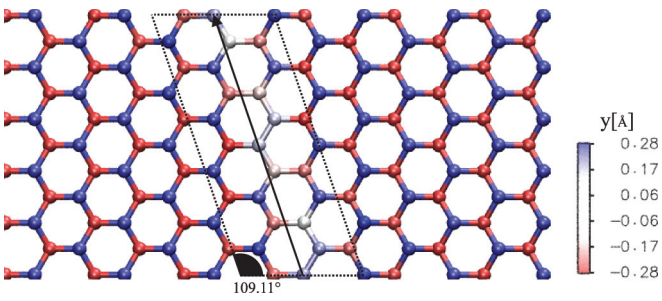

FIG. 5. (Color online) Geometry for a chiral line defect. The angle between the defect direction and the pure zigzag direction is 19.11°. Here, the atoms are colored according to their out-of-plane dislocation. The arrow represents the lattice vector along the defect direction.

It is important to stress that the values presented in Table I are one order of magnitude lower when compared to either grain boundaries or dislocation linear defects in graphene.[25,26] This is a consequence of the fact that grain boundaries in graphene always involve a chemical bond reconstruction, and the hexagons are converted in other polygons, like pentagons and heptagons. This kind of reconstruction highly increases the formation energy of the linear defects in graphene. On the other hand, as reported in this paper, the linear defects in silicene may be generated by another mechanism: an out-of-plane dislocation rearrangement, leading to lower values of the formation energy and, thus, a defect more likely to be created.

E. Adsorption of gold atoms

Another interesting point related to these line defects is that they might be preferential adsorption sites. To investigate this question, we performed proof-of-concept simulations with a single gold atom adsorbed over the system. In these simulations we used supercells in which the Au atoms are separated by more than 18 Å from their periodic images. This is necessary to sufficiently decrease the interaction between the Au atom and its images. We choose Au atoms because there are previous experiments of single atom adsorption over the Si(100) surface,[28] which bear some similarities with the line defects we propose due to the presence of dimers. Furthermore, gold is frequently used in nanodevices.

Considering a single gold atom over the pristine silicene, we found a binding energy (E_b) of -3.50 eV when adsorbed at the hollow site. This adsorption site is energetically favorable by 0.38 and 0.66 eV when compared to the top and bridge configurations, respectively. Corroborating previous works, this binding energy indicates a much stronger bond in silicene when compared to graphene.[16,29–32] To investigate the adsorption of Au over the buckling interfaces we considered several adsorption sites, and the energetically most favorable ones for each one of the four interfaces are shown in Fig. 6. In the same figure we also present E_b for each one of these configurations. Confirming our expectations, the results show that all these defects are more reactive than the pristine region, indicating that they will be preferential absorption sites. This opens up a variety of possibilities for nanoengineering, where via adsorption of particular atoms or molecules at these sites one can tailor the properties of one-dimensional channels embedded on the silicene sheet.

IV. CONCLUSIONS

In conclusion, we have shown that due to the buckling structure of silicene it is possible to have a new kind of low-energy grain boundary associated with the reversal of the buckling phase, contrary to graphene, where the grain boundary defects always have high energy. In particular, we have investigated in detail these buckling phase interfaces, showing the following:

(i) Modifications in the density of states will appear far from the Fermi energy.

(ii) The formation energies of these interfaces are very low, of the order of $(k_B T_{300\,\mathrm{K}})/\text{Å}$. These values are approximately one order of magnitude lower than grain boundaries in graphene.

(iii) These structures can be experimentally identified by STM images.

(iv) These interfaces are preferential adsorption sites when compared to the pristine region. Therefore, these interfaces are important and most likely common defects in silicene, and they may be thus used to control the adsorption of atoms and molecules, which could lead to many possibilities in molecular engineering.

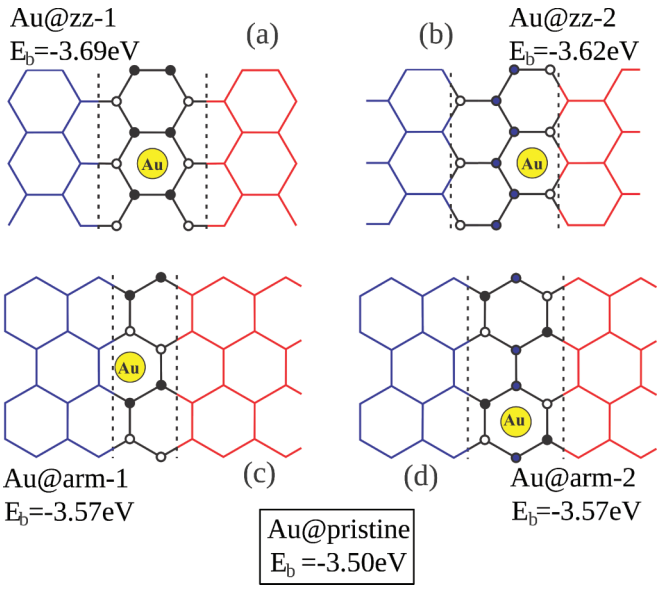

FIG. 6. (Color online) Schematic representation of the most stable adsorption site of Au over the (a) zz-1, (b) zz-2, (c) arm-1, and (d) arm-2 interfaces.

ACKNOWLEDGMENTS

We would like to thank the Conselho Nacional de Desenvolvimento Científico e Tecnológico/Institutos Nacionais de Ciência e Tecnologia do Brasil (CNPq/INCT), the Coordenação de Aperfeiçoamento de Pessoal de Nível Superior (CAPES), and the Fundação de Amparo à Pesquisa do Estado de São Paulo (FAPESP).

APPENDIX A: HAMILTONIAN MATRIX ELEMENTS FOR THE TIGHT-BINDING MODEL OF THE BUCKLING PHASE INTERFACES

In this appendix we explicitly show the matrix elements for the effective model used to study the buckling phase inversion in silicene. We first construct the Hamiltonian for the pristine silicene with a large supercell, and we then simulate the buckling inversion line defects by changing the on-site energy only for specific sites.

For the pristine silicene, we construct a simple nearest-neighbor tight-binding Hamiltonian with one effective orbital per site, with rectangular supercells having the smallest possible size along the defect direction ($\hat{\mathbf{z}}$) and an arbitrary size along the lateral direction ($\hat{\mathbf{x}}$). For both zigzag and armchair directions we used building blocks with four sites, as shown

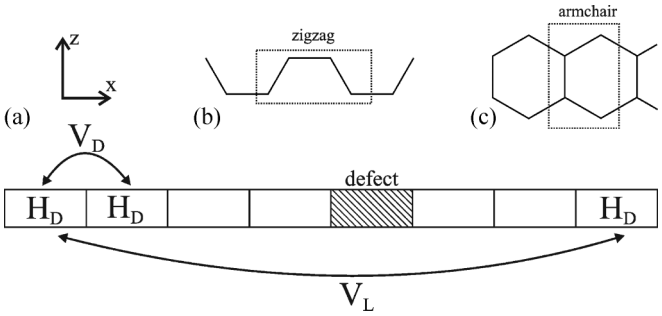

FIG. 7. (a) Diagrammatic representation of the Hamiltonian coupling terms. (b) and (c) Building blocks for the zigzag and armchair structures, enclosed with dashed lines.

in Figs. 7(b) and 7(c), respectively. Thus, the total pristine Hamiltonian can be written as

$$H(k_x,k_y) = \begin{pmatrix} H_D & V_D & 0 & 0 & \cdots & V_L \\ V_D^\dagger & H_D & V_D & 0 & \cdots & 0 \\ 0 & V_D^\dagger & H_D & V_D & & 0 \\ \vdots & & & \ddots & & \\ & & & & & \\ V_L^\dagger & 0 & \cdots & 0 & V_D^\dagger & H_D \end{pmatrix}. \quad \text{(A1)}$$

Here, H_D is the building block Hamiltonian, V_D is the coupling between neighboring building blocks, and V_L is the coupling between neighboring supercells. A diagrammatic representation of these interactions is shown in Fig. 7(a). Since the building blocks have four sites, all these are 4×4 matrices. Particularly, for the armchair direction these terms are given by

$$H_D = -t \begin{pmatrix} 0 & e^{-ik_z} & 1 & 0 \\ e^{ik_z} & 0 & 0 & 1 \\ 1 & 0 & 0 & 1 \\ 0 & 1 & 1 & 0 \end{pmatrix}, \quad \text{(A2)}$$

$$V_D = -t \begin{pmatrix} 0 & 0 & 0 & 0 \\ 0 & 0 & 0 & 0 \\ 1 & 0 & 0 & 0 \\ 0 & 1 & 0 & 0 \end{pmatrix}, \quad \text{(A3)}$$

$$V_L = -t \begin{pmatrix} 0 & 0 & e^{-ik_x} & 0 \\ 0 & 0 & 0 & e^{ik_x} \\ 0 & 0 & 0 & 0 \\ 0 & 0 & 0 & 0 \end{pmatrix}, \quad \text{(A4)}$$

where t is the transfer integral and k_z (k_x) is the crystalline momentum along (perpendicular to) the defect direction. For the zigzag direction, the Hamiltonian building block terms are written as

$$H_D = -t \begin{pmatrix} 0 & c_k & 0 & 0 \\ c_k^* & 0 & 1 & 0 \\ 0 & 1 & 0 & c_k^* \\ 0 & 0 & c_k & 0 \end{pmatrix}, \quad \text{(A5)}$$

$$V_D = -t \begin{pmatrix} 0 & 0 & 0 & 0 \\ 0 & 0 & 0 & 0 \\ 0 & 0 & 0 & 0 \\ 1 & 0 & 0 & 0 \end{pmatrix}, \quad \text{(A6)}$$

$$V_L = -t \begin{pmatrix} 0 & 0 & 0 & e^{-ik_x} \\ 0 & 0 & 0 & 0 \\ 0 & 0 & 0 & 0 \\ 0 & 0 & 0 & 0 \end{pmatrix}. \quad \text{(A7)}$$

Here, $c_k = (1 + e^{ik_z})$ is an effective coupling term. Note that $c_k \to 0$ when $k_z \to \pi$, as discussed in Sec. III B.

The rehybridization of the defect sites leads to changes in their on-site energy. Therefore, to simulate a single line defect it is necessary to change the on-site energies (considered zero for the pristine sites) for a single building block, as schematically shown in Fig. 7(a).

APPENDIX B: OSCILLATIONS IN THE DENSITY OF STATES OF DEFECTS IN THE ARMCHAIR DIRECTION

The density of states (DOS) of these buckled line defects could present some oscillations when compared to the silicene without any defect. This feature occurs with both DFT and tight-binding calculations. This behavior is illustrated in Fig. 8, where we present the DOS for the arm-2 defect. In this figure, we compare the DOS calculated with a small supercell having 40 sites (same defect-defect distance present in the *ab initio* calculations) with a DOS obtained with a system ten times bigger ($N = 400$). In the latter system the line defects are separated by 48 nm from its periodic image, and in fact there is no interaction between them. As a consequence, the wave function presented in Fig. 8(b) decays to zero before having any overlapping with the wave function of the neighbor line defect. In this case the DOS is almost indistinguishable when compared to the pristine case. On the other hand, for the smaller

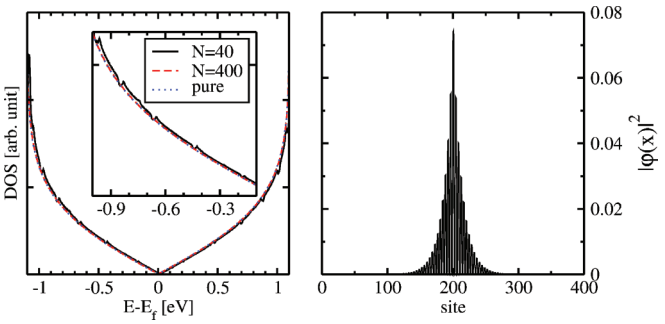

FIG. 8. (Color online) (a) Density of states (DOS) of silicene with the arm-2 defect varying the distance between the line defect and its lateral image. For $N = 40$ the distance is 3.8 nm, whereas for $N = 400$ the distance is 38 nm. We normalize the absolute value or the DOS by the respective number of sites of the system. Inset: Zoom of the DOS. Also considering the arm-2 defect we show in (b) the modulus square of the wave function of the valence band at $k_x = 0$ and $k_z = \pi$. Here, the system has 400 sites ($N = 400$). The defect lies in sites 201–204.

supercell ($N = 40$), the distance between the defect and its periodic image is 3.8 nm. Thus, there is an overlap between the wave functions localized at the defect and its periodic image, leading to the appearance of several small spurious oscillations in the DOS. It is important to stress that this interaction does not affect any of our main conclusions.

*mplima@if.usp.br
†fazzio@if.usp.br
‡jose.roque@lnls.br

[1] H. Sahaf, L. Masson, C. Léandri, B. Aufray, G. Le Lay, and F. Ronci, Appl. Phys. Lett. **90**, 263110 (2007).
[2] K. S. Novoselov, A. K. Geim, S. V. Morozov, D. Jiang, Y. Zhang, S. V. Dubonos, I. V. Grigorieva, and A. A. Firsov, Science **306**, 666 (2004).
[3] B. Lalmi, H. Oughaddou, H. Enriquez, A. Kara, S. Vizzini, B. Ealet, and B. Aufray, Appl. Phys. Lett. **97**, 223109 (2010).
[4] C. L. Lin, R. Arafune, K. Kawahara, N. Tsukahara, E. Minamitani, Y. Kim, N. Takagi, and M. Kawai, Appl. Phys. Express **5**, 045802 (2012).
[5] H. Jamgotchian, Y. Colignon, N. Hamzaoui, B. Ealet, J. Y. Hoarau, B. Aufray, and J. P. Biberian, J. Phys.: Condens. Matter **24**, 172001 (2012).
[6] B. Feng, Z. Ding, S. Meng, Y. Yao, X. He, P. Cheng, L. Chen, and K. Wu, Nano Lett. **12**, 3507 (2012).
[7] A. Fleurence, R. Friedlein, T. Ozaki, H. Kawai, Y. Wang, and Y. Yamada-Takamura, Phys. Rev. Lett. **108**, 245501 (2012).
[8] P. Vogt, P. De Padova, C. Quaresima, J. Avila, E. Frantzeskakis, M. C. Asensio, A. Resta, B. Ealet, and G. Le Lay, Phys. Rev. Lett. **108**, 155501 (2012).
[9] K. Takeda and K. Shiraishi, Phys. Rev. B **50**, 14916 (1994).
[10] G. G. Guzmán-Verri and L. C. Lew Yan Voon, Phys. Rev. B **76**, 075131 (2007).
[11] A. Kara, H. Enriquez, A. P. Seitsonen, L. C. L. Y. Voon, S. Vizzini, B. Aufray, and H. Oughaddou, Surf. Science Rep. **67**, 1 (2012).
[12] C. C. Liu, W. Feng, and Y. Yao, Phys. Rev. Lett. **107**, 076802 (2011); C. C. Liu, H. Jiang, and Y. Yao, Phys. Rev. B **84**, 195430 (2011).
[13] Z. Ni, Q. Liu, K. Tang, J. Zheng, J. Zhou, R. Qin, Z. Gao, D. Yu, and J. Lu, Nano Lett. **12**, 113 (2012).
[14] N. D. Drummond, V. Zólyomi, and V. I. Fal'ko, Phys. Rev. B **85**, 075423 (2012).
[15] M. Ezawa, New J. Phys. **14**, 033003 (2012).
[16] X. Lin and J. Ni, Phys. Rev. B **86**, 075440 (2012).
[17] E. Artacho, D. Sánchez-Portal, P. Ordejón, A. García, and J. M. Soler, Phys. Status Solidi B **215**, 809 (1999).
[18] J. P. Perdew and A. Zunger, Phys. Rev. B **23**, 5048 (1981).
[19] S. Cahangirov, M. Topsakal, E. Aktürk, H. Sahin, and S. Ciraci, Phys. Rev. Lett. **102**, 236804 (2009).
[20] S. Wang, Phys. Chem. Chem. Phys. **13**, 11929 (2011).
[21] We have also studied an intermediate chiral configuration (see Fig. 5). Since this geometry has higher energy than either the zigzag or armchair, as shown in Table I, we do not analyze it in detail.
[22] We have also locally changed the value of the transfer integral at the defect without any appreciable changes in the band structure.
[23] J. Tersoff and D. R. Hamann, Phys. Rev. B **31**, 805 (1985).
[24] L. Meng, Y. L. Wang, L. Z. Zhang, S. X. Du, R. T. Wu, L. F. Li, Y. Zhang, G. Li, H. T. Zhou, W. A. Hofer, A. Werner, and H. J. Gao, Nano Lett. **13**, 685 (2013).
[25] O. V. Yazyev and S. G. Louie, Nature Mat. **9**, 806 (2010).
[26] O. V. Yazyev and S. G. Louie, Phys. Rev. B **81**, 195420 (2010).
[27] L. Chen, H. Li, B. Feng, Z. Ding, J. Qiu, P. Cheng, K. Wu, and S. Meng, Phys. Rev. Lett. **110**, 085504 (2013).
[28] F. Chiaravalloti, D. Riedel, G. Dujardin, H. P. Pinto, and A. S. Foster, Phys. Rev. B **79**, 245431 (2009).
[29] M. P. Lima, A. J. R. da Silva, and A. Fazzio, Phys. Rev. B **84**, 245411 (2011).
[30] M. Amft, S. Lebègue, O. Eriksson, and N. V. Skorodumova, J. Phys.: Condens. Matter **23**, 395001 (2011).
[31] W. H. Brito, R. Kagimura, and R. H. Miwa, Phys. Rev. B **85**, 035404 (2012).
[32] W. H. Brito, R. Kagimura, and R. H. Miwa, Appl. Phys. Lett. **98**, 213107 (2011).